Cell Reports Medicine, Volume *5*

Supplemental information

Targeting PDGF signaling of cancer-associated fibroblasts blocks feedback activation of HIF-1α and tumor progression of clear cell ovarian cancer

Yutaro Mori, Yoshie Okimoto, Hiroaki Sakai, Yusuke Kanda, Hirokazu Ohata, Daisuke Shiokawa, Mikiko Suzuki, Hiroshi Yoshida, Haruka Ueda, Tomoyuki Sekizuka, Ryo Tamura, Kaoru Yamawaki, Tatsuya Ishiguro, Raul Nicolas Mateos, Yuichi Shiraishi, Yasushi Yatabe, Akinobu Hamada, Kosuke Yoshihara, Takayuki Enomoto, and Koji Okamoto

Mori et al. Figure S1

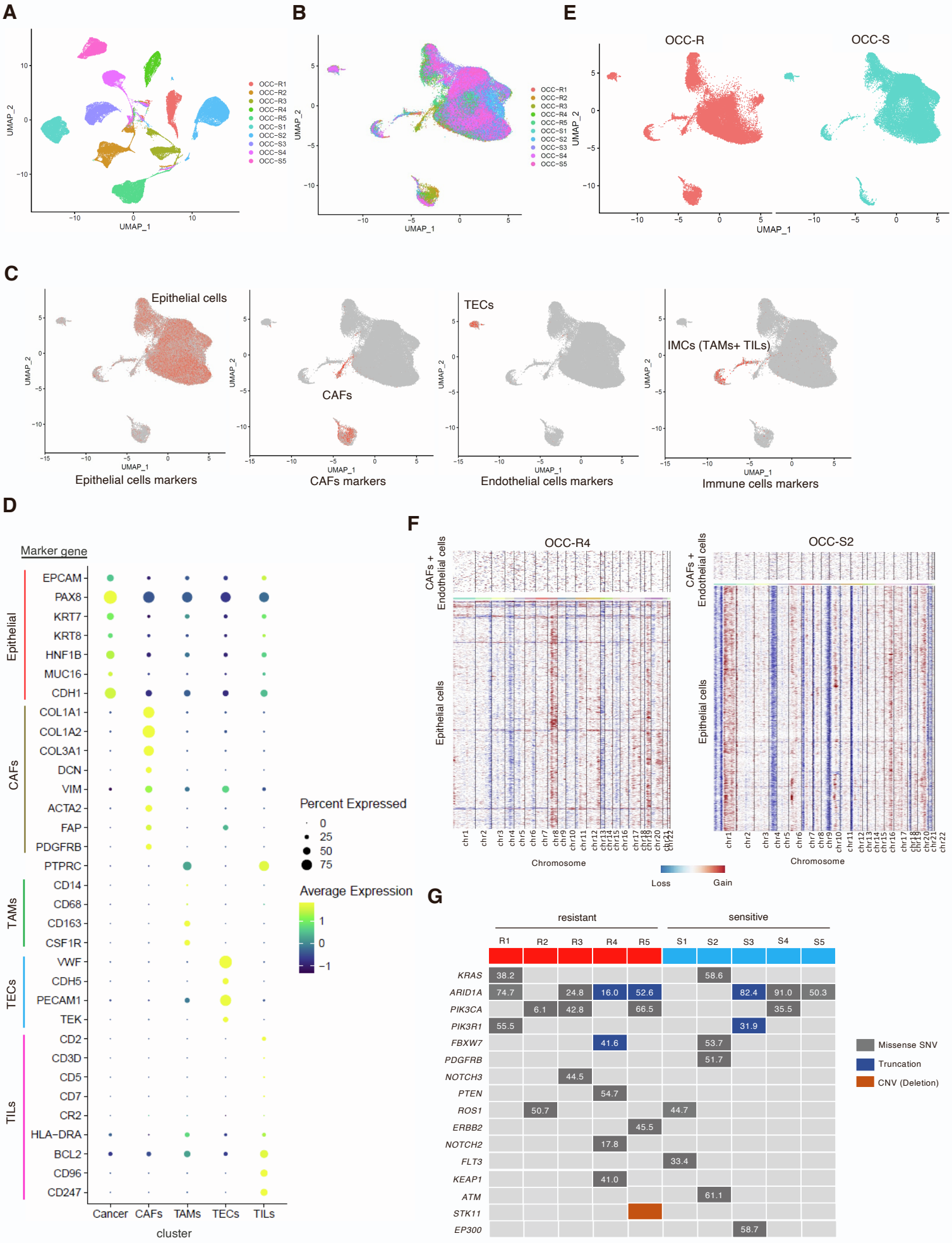

Figure S1. Identification of cancer subpopulations associated with chemoresistance of OCCC. Related to Figure 1.

(A) UMAP plot of chemoresistant (OCC-R) and chemosensitive (OCC-S) OCCC cells that passed quality control and were color-labeled according to the indicated clinical cases.

(B) Original snRNA-seq data from OCCC cases were subjected to an anchoring procedure, and the integrated datasets were used to generate the UMAP plot.

(C) Feature plots on the integrated UMAP showing expression of marker genes of each population. Expression of representative markers of epithelial cells (*EPCAM*, *PAX8*, *KRT7*), CAFs (*COL1A1*, *COL1A2*, *DCN*, *VIM*), endothelial cells (TECs) (*VWF*, *CDH5*, *PECAM1*), and immune cells (IMCs (TAMs +TILs)) (*PTPRC*) are shown.

(D) Dot plots of expression of marker genes in the indicated cell types.

(E) UMAP of OCCC cells, color-labeled according to chemoresistant and chemosensitive cases.

(F) Heatmap of copy-number alterations inferred from snRNA-seq data (OCC-R4 and OCC-S2) based on the average relative expression of 100 genes within sliding windows. Rows in the upper and lower panels correspond to non-tumor cells (CAFs + endothelial cells) and epithelial cells, respectively. Data from non-tumor cells were used as a reference.

(G) Genomic alterations in OCCC tumors. Colors indicate the type of genomic alteration. The numbers in the box represent the variance rate of each gene mutation (%).

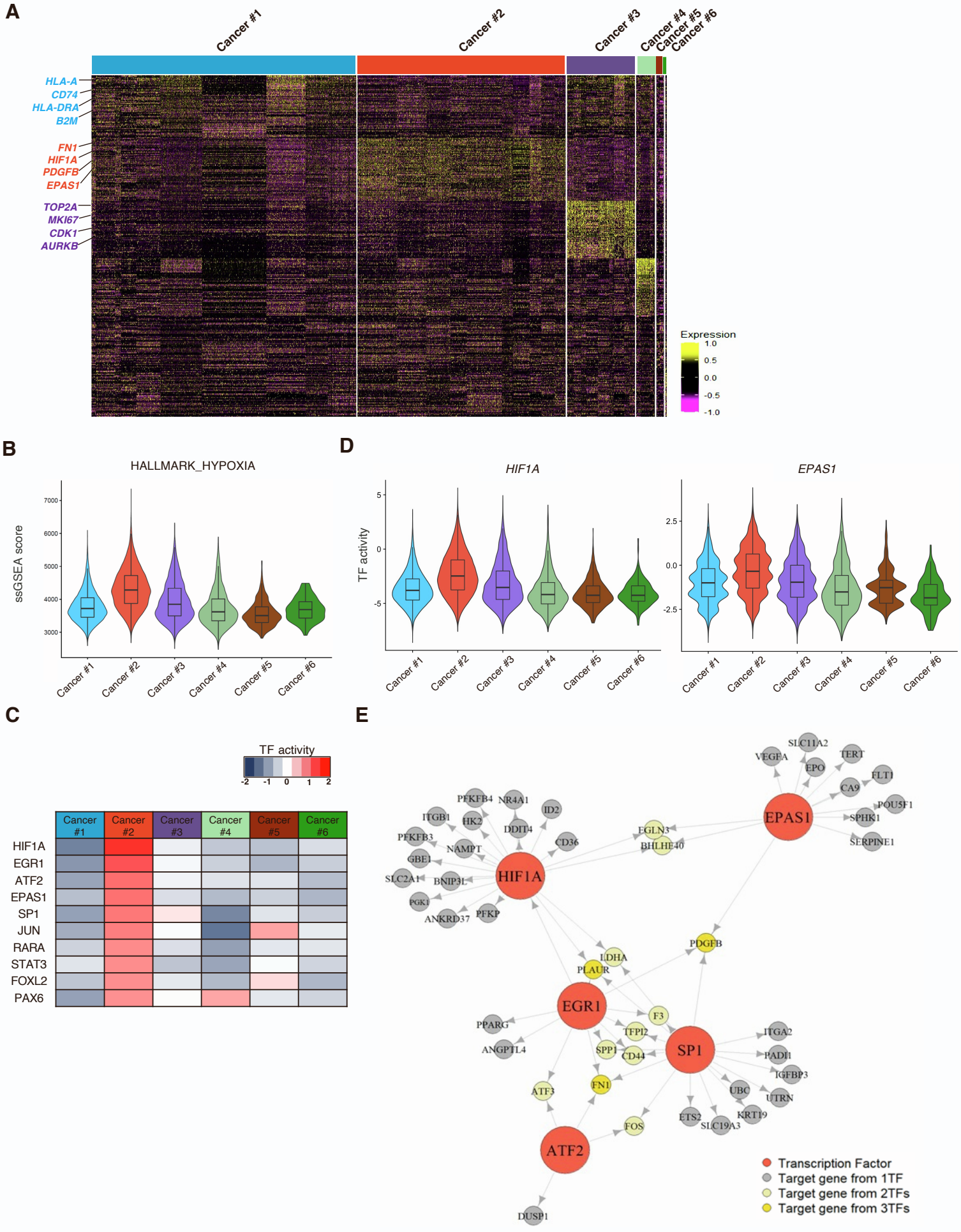
A
Cancer #1
Cancer #2
Cancer #3
Cancer #4
Cancer #5
Cancer #6
HLA-A
CD74
HLA-DRA
B2M
FN1
HIF1A
PDGFB
EPAS1
TOP2A
MKI67
CDK1
AURKB
Expression
1.0
0.5
0.0
-0.5
-1.0
B
HALLMARK_HYPOXIA
ssGSEA score
7000
6000
5000
4000
3000
Cancer #1
Cancer #2
Cancer #3
Cancer #4
Cancer #5
Cancer #6
D
HIF1A
EPAS1
TF activity
5
0
-5
2.5
0.0
-2.5
C
TF activity
-2
-1
0
1
2
Cancer #1
Cancer #2
Cancer #3
Cancer #4
Cancer #5
Cancer #6
HIF1A
EGR1
ATF2
EPAS1
SP1
JUN
RARA
STAT3
FOXL2
PAX6
E
SLC11A2
VEGFA
TERT
EPO
FLT1
CA9
POU5F1
SPHK1
SERPINE1
EPAS1
PFKFB4
NR4A1
ID2
ITGB1
HK2
DDIT4
PFKFB3
NAMPT
CD36
GBE1
SLC2A1
BNIP3L
HIF1A
PGK1
ANKRD37
PFKP
EGLN3
BHLHE40
PDGFB
LDHA
PLAUR
EGR1
PPARG
ANGPTL4
F3
TFPI2
SPP1
CD44
SP1
ITGA2
PADI1
IGFBP3
ATF3
FN1
UBC
UTRN
ETS2
KRT19
SLC19A3
FOS
ATF2
DUSP1
Transcription Factor
Target gene from 1TF
Target gene from 2TFs
Target gene from 3TFs

Figure S2. Chemoresistant population of OCCC is associated with HIF activation and poor prognosis. Related to Figure 2.

(A) Heatmap of top-ranking genes in each subpopulation. Representative genes in the Cancer #1–3 subpopulations are shown.

(B) Violin plots of hallmark-hypoxia signature scores for the indicated cancer subpopulations.

(C) Heatmap of transcription factor (TF) activity, as inferred by the VIPER algorism, in the indicated cancer subpopulations. The 10 top-ranked TF genes in the Cancer #2 subpopulation are shown.

(D) Violin plots of HIF1A and EPAS1(HIF2A) TF activity in the indicated cancer subpopulations.

(E) Schematic representation of a regulatory network of TFs and their downstream genes that are activated in the Cancer #2 subpopulation. TFs activated in the Cancer #2 subpopulation are denoted by large red circles, and their target genes (listed in DoRothEA) are denoted by small circles. Target genes regulated by one, two, or three TFs are shown in gray, cream-yellow, or orange, respectively.

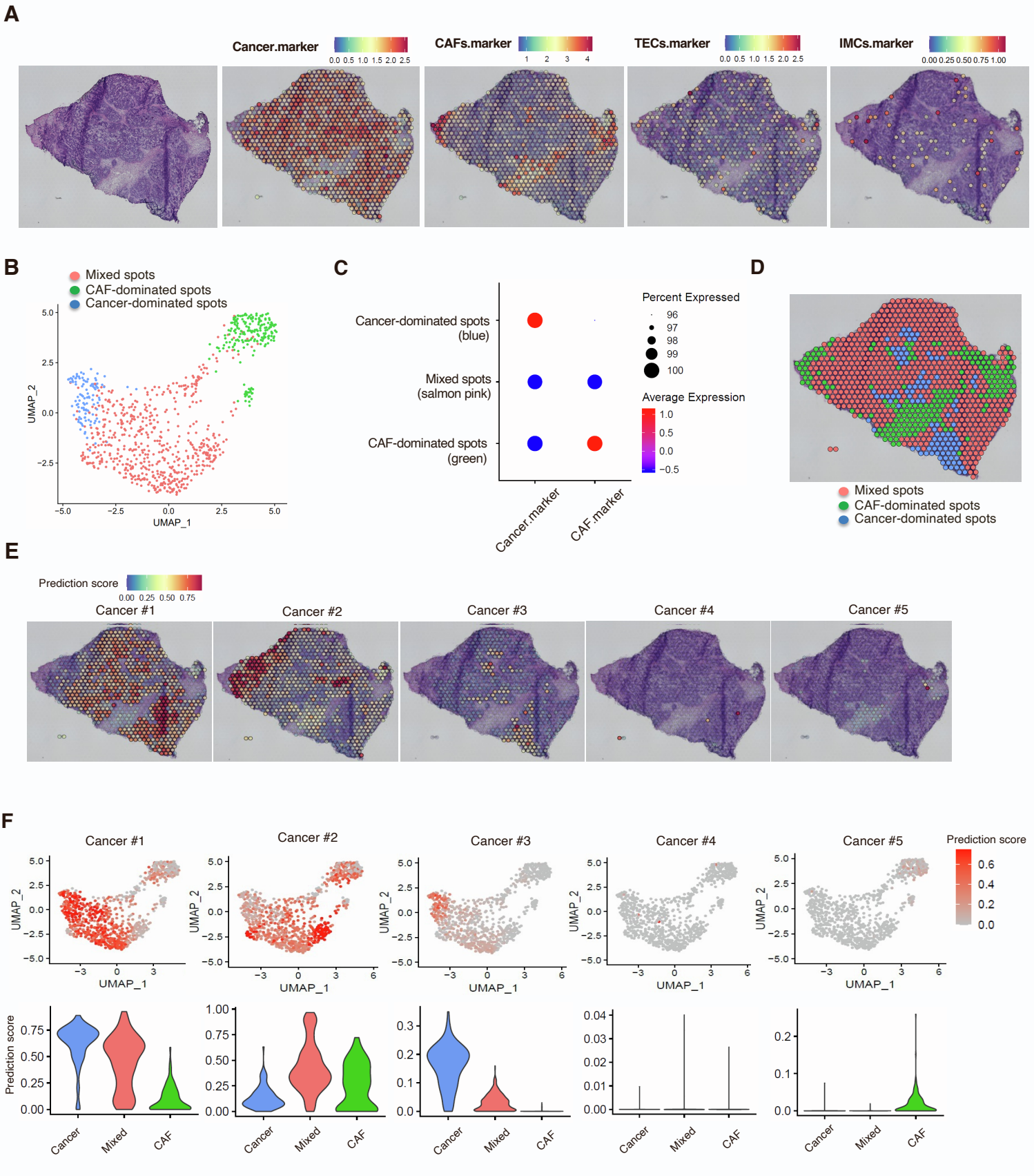
A
Cancer.marker
0.0 0.5 1.0 1.5 2.0 2.5
CAFs.marker
1 2 3 4
TECs.marker
0.0 0.5 1.0 1.5 2.0 2.5
IMCs.marker
0.00 0.25 0.50 0.75 1.00
B
Mixed spots
CAF-dominated spots
Cancer-dominated spots
UMAP_2
UMAP_1
C
Cancer-dominated spots (blue)
Mixed spots (salmon pink)
CAF-dominated spots (green)
Cancer.marker
CAF.marker
Percent Expressed
96
97
98
99
100
Average Expression
1.0
0.5
0.0
−0.5
D
Mixed spots
CAF-dominated spots
Cancer-dominated spots
E
Prediction score
0.00 0.25 0.50 0.75
Cancer #1
Cancer #2
Cancer #3
Cancer #4
Cancer #5
F
Cancer #1
Cancer #2
Cancer #3
Cancer #4
Cancer #5
Prediction score
0.6
0.4
0.2
0.0
UMAP_2
UMAP_1
Prediction score
Cancer
Mixed
CAF

Figure S3. Chemoresistant cells are localized in CAF-populated areas of OCCC. Related to Figure 3.

(A) (far left) H&E staining of OCC-S3 tissue sections. (right) ST spots on H&E-stained sections were overlaid with spatial feature plots of ovarian cancer cell markers (*EPCAM*, *PAX8*, *KRT7*), CAF markers (*COL1A1*, *COL1A2*, *DCN*, *VIM*), endothelial cell (TEC) markers (*VWF*, *CDH5*, *PECAM1*), or an immune cell (IMC) marker (*PTPRC*).

(B) UMAP plots of the ST spots shown in a. ST spots were classified into three clusters by unsupervised clustering, and denoted by different colors.

(C) Dot plots showing average expression of CAF markers and ovarian cancer cell markers in the indicated clusters. Three clusters shown in B were designated as cancer-dominated spots, CAF-dominated spots, and Mixed spots, based upon marker expression.

(D) Spatial presentation of the three cluster in OCC-S3 tissue sections. Tissue localization of the clustered ST spots was visualized and denoted by the indicated colors.

(E) Spatial feature plots of the prediction scores for the indicated cancer subpopulations (Cancer #1–5) in OCC-S3 tissue sections.

(F) Top: UMAP feature plots of ST spots of OCC-S3. Prediction scores for the indicated cancer subpopulations are shown in red. Bottom: Violin plots of the prediction scores for cancer subpopulations shown in the top columns. ST spots were classified into three groups as shown in d, and prediction scores for each group are presented.

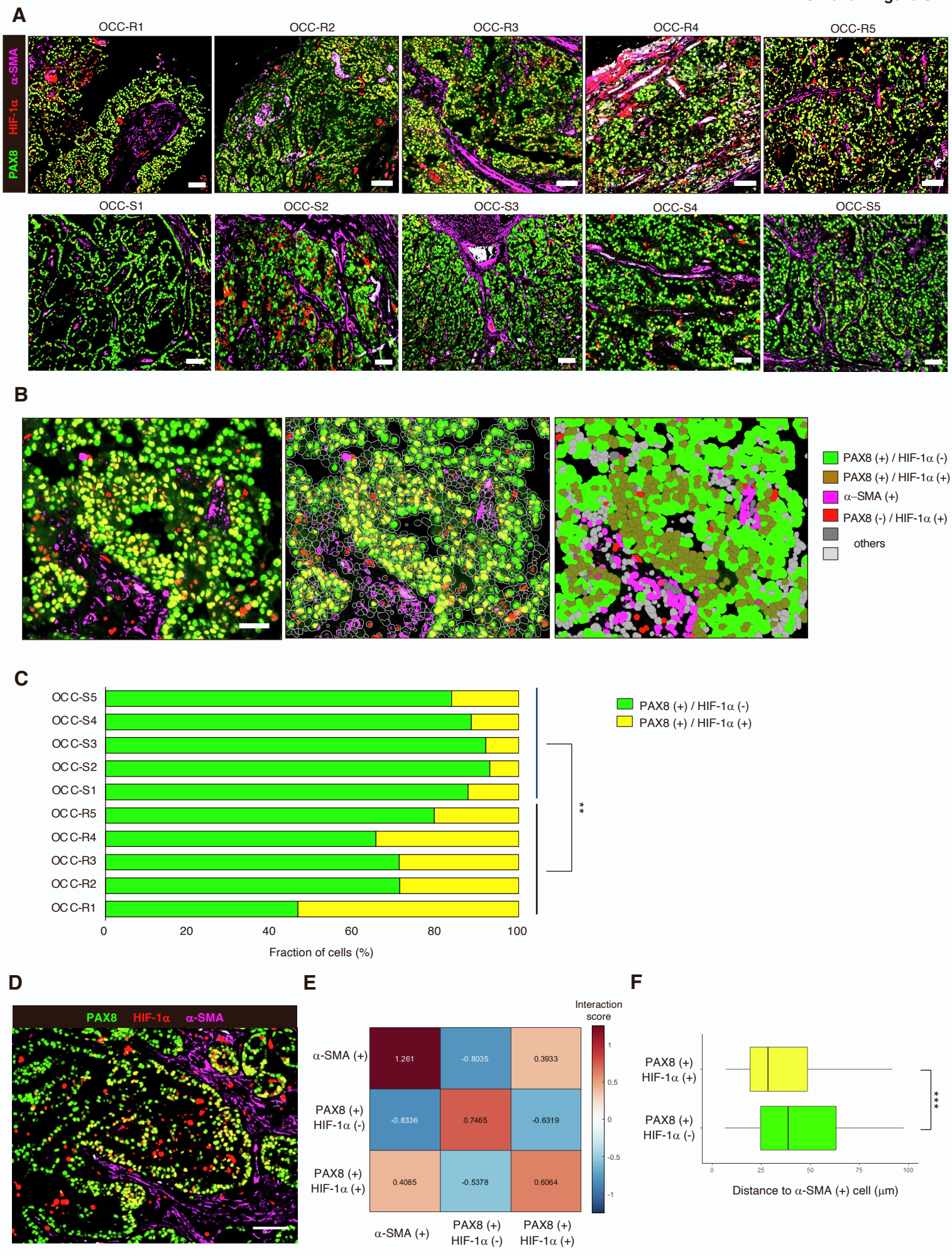
A
OCC-R1
OCC-R2
OCC-R3
OCC-R4
OCC-R5
PAX8
HIF-1α
α-SMA
OCC-S1
OCC-S2
OCC-S3
OCC-S4
OCC-S5
B
PAX8 (+) / HIF-1α (-)
PAX8 (+) / HIF-1α (+)
α–SMA (+)
PAX8 (-) / HIF-1α (+)
others
C
OCC-S5
OCC-S4
OCC-S3
OCC-S2
OCC-S1
OCC-R5
OCC-R4
OCC-R3
OCC-R2
OCC-R1
0
20
40
60
80
100
Fraction of cells (%)
**
PAX8 (+) / HIF-1α (-)
PAX8 (+) / HIF-1α (+)
D
PAX8
HIF-1α
α-SMA
E
Interaction score
α-SMA (+)
PAX8 (+) HIF-1α (-)
PAX8 (+) HIF-1α (+)
1.261
-0.8035
0.3933
-0.8336
0.7465
-0.6319
0.4085
-0.5378
0.6064
1
0.5
0
-0.5
-1
α-SMA (+)
PAX8 (+) HIF-1α (-)
PAX8 (+) HIF-1α (+)
F
PAX8 (+) HIF-1α (+)
PAX8 (+) HIF-1α (-)
***
0
25
50
75
100
Distance to α-SMA (+) cell (μm)

Figure S4. HIF-1α-expressing cancer cells reside near CAFs in chemoresistant OCCC. Related to Figure 3.

(A) Representative images of co-immunostaining of chemosensitive and chemoresistant tumors with HIF-1α (Red), PAX8 (Green), and α-SMA (Pink). Scale bar, 100 μm.

(B) Segmented cells were annotated by the image processing algorithm in QuPath. (Left) A representative image of coimmunostaining of chemoresistant tumor (OCC-R2). (Middle) Cell segmentation. (Right) Annotation of segmented cells based upon immunostaining.

(C) Percentage of HIF-1α(+) cancer cells (calculated from whole-slide images of tumor sections). $^{**}p < 0.01$.

(D) Representative magnified images of HIF-1α(+) cancer cells near to α-SMA (+) CAF in a chemoresistant tumor (OCC-R2). Scale bar, 100 mm.

(E) Nearest neighbor analysis of the image shown in D.

(F) Box plot of average distance from PAX8(+)/HIF-1α(+) cells or PAX8(+)/HIF-1α(-) cells to the nearest α-SMA(+) cells, calculated from the image shown in D. *P* values were determined by Student's t test. Statistically significant differences are indicated: $^{***}p < 0.001$.

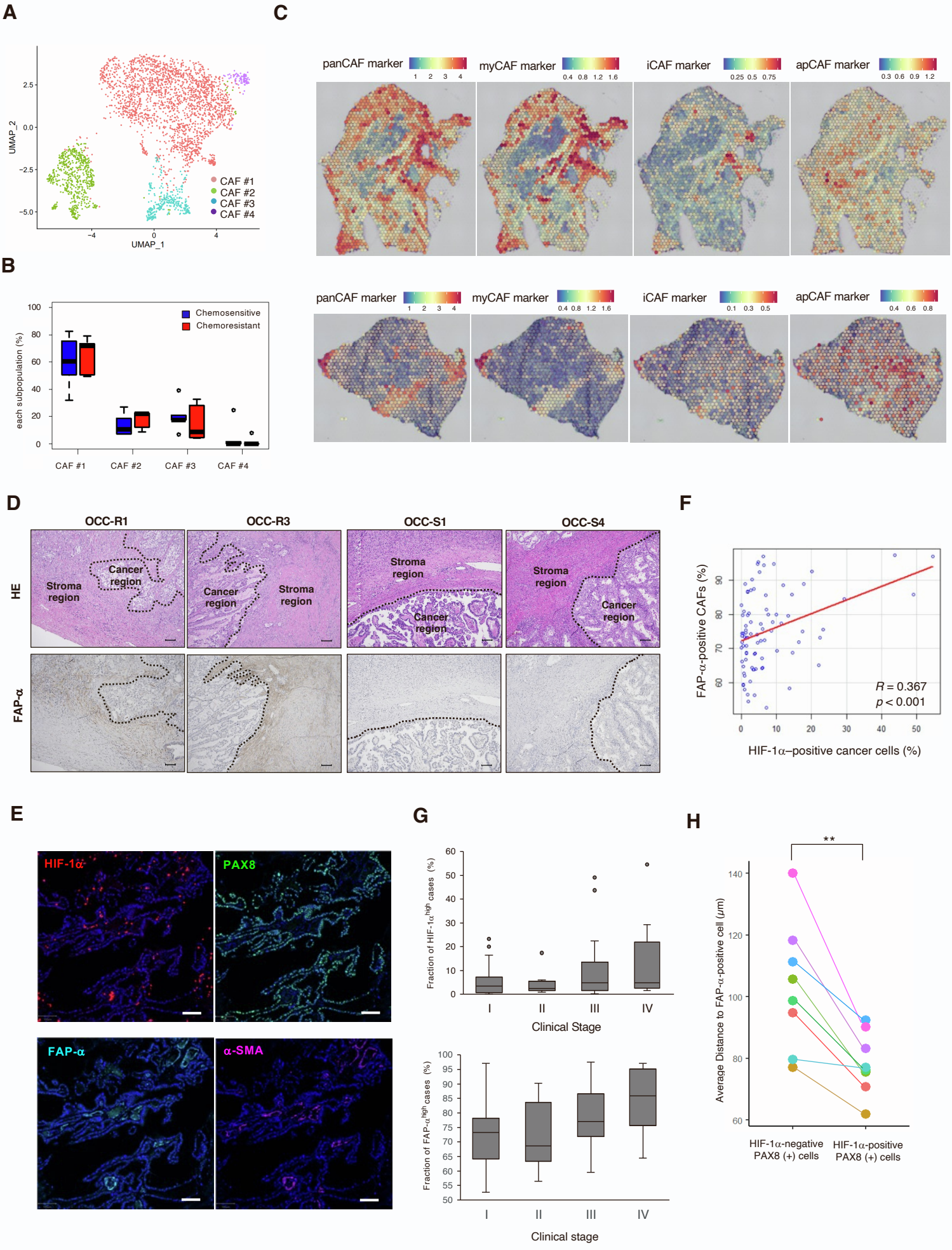
A
UMAP_2
UMAP_1
CAF #1
CAF #2
CAF #3
CAF #4
B
each subpopulation (%)
Chemosensitive
Chemoresistant
CAF #1
CAF #2
CAF #3
CAF #4
C
panCAF marker
myCAF marker
iCAF marker
apCAF marker
D
OCC-R1
OCC-R3
OCC-S1
OCC-S4
HE
FAP-α
Stroma region
Cancer region
E
HIF-1α
PAX8
FAP-α
α-SMA
F
FAP-α-positive CAFs (%)
HIF-1α–positive cancer cells (%)
R = 0.367
p < 0.001
G
Fraction of HIF-1α high cases (%)
Fraction of FAP-α high cases (%)
Clinical Stage
Clinical stage
I
II
III
IV
H
Average Distance to FAP-α-positive cell (μm)
**
HIF-1α-negative PAX8 (+) cells
HIF-1α-positive PAX8 (+) cells

Figure S5. CAFs in chemoresistant tumors are associated with myofibroblastic phenotype. Related to Figure 4.

(A) UMAP plot of the OCCC CAFs shown in Fig. 5a, color-coded into four subpopulations (CAF #1–4) by unsupervised clustering.

(B) Box plots of percentage of the indicated CAF subpopulations from the chemoresistant and chemosensitive tumors shown in A.

(C) Spatial feature plots of panCAF markers, myCAF markers, iCAF markers, and apCAF markers in OCC-R2 (top) and OCC-S3 (bottom) tissue sections.

(D) H&E images and immunostaining with FAP-α in indicated chemoresistant and chemosensitive tumors. Dotted lines depict the boundary between the tumor and the stroma regions. Scale bar: 100 μm.

(E) Representative immunostaining with HIF-1α, PAX8, α-SMA, or FAP-α by Vectra Polaris multi-color imaging system. Scale bar: 100 μm.

(F) Fraction of HIF-1α-positive cancer cells and FAP-α-positive CAFs in 86 cases of OCCC. Correlation between the percentage of HIF-1α-positive cancer cells and FAP-α-positive CAFs was determined by calculating Pearson's correlation coefficient.

(G) Percentage of HIF-1α^{high} and FAP-α^{high} cases in each stage. Stage I (n=45), Stage II (n=8), Stage III (n=24), and Stage IV (n=9). Top and bottom end of the boxes represent 25% and 75% percentile, respectively, and horizontal bars in the box indicate median values.

(H) Dot plot showing average distances from FAP-α-positive cell to nearest HIF-1α-positive or HIF-1α-negative cell. Multi-color fluorescent images of HIF-1α^{high}/FAP-α^{high} samples (n=8) were used to calculate the average distances as described in the Method section. The same samples share identical color. *p*-values were determined by student t-test. ** $p < 0.01$.

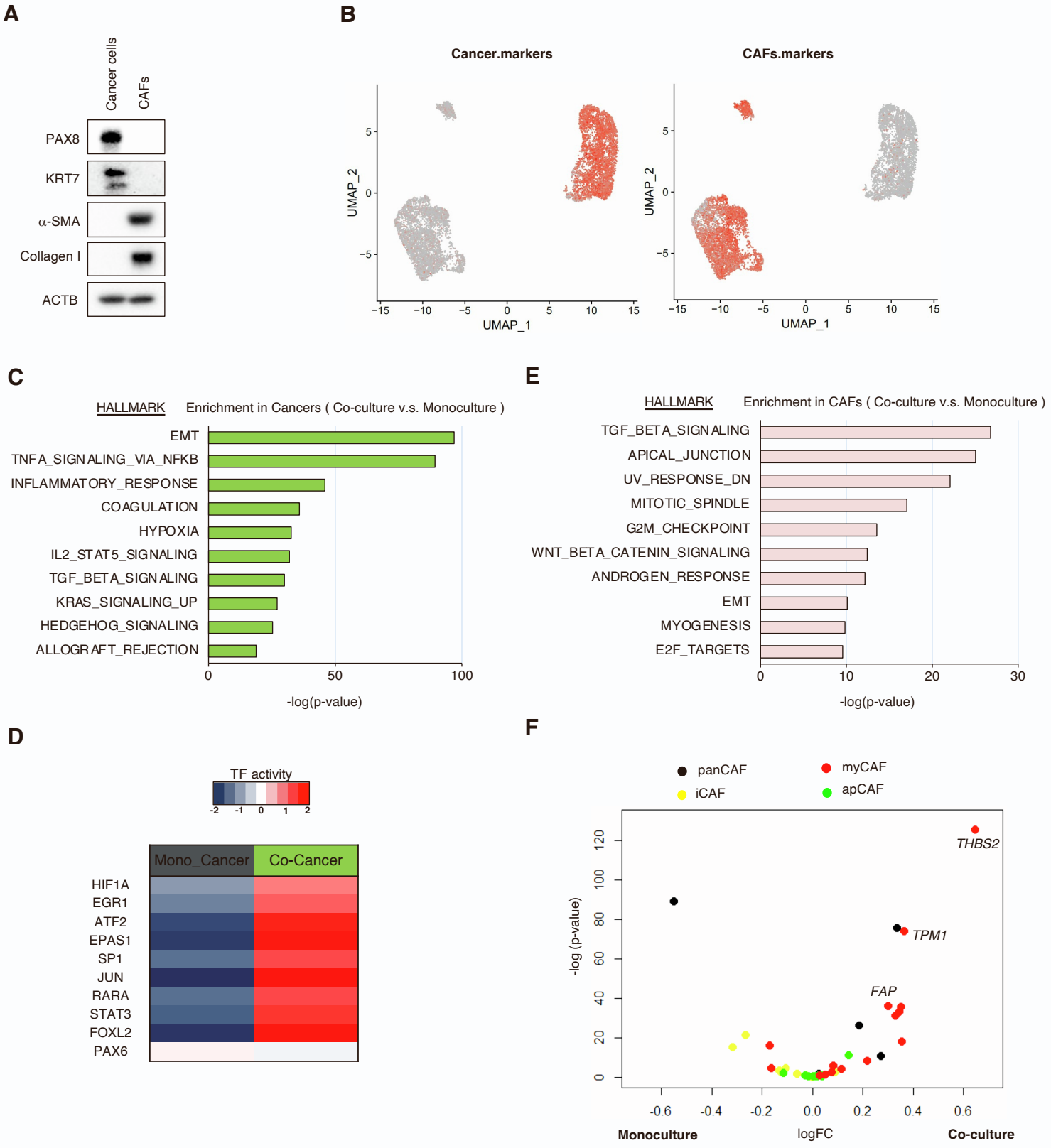
A
Cancer cells
CAFs
PAX8
KRT7
α-SMA
Collagen I
ACTB
B
Cancer.markers
CAFs.markers
UMAP_2
UMAP_1
C
HALLMARK Enrichment in Cancers (Co-culture v.s. Monoculture)
EMT
TNFA_SIGNALING_VIA_NFKB
INFLAMMATORY_RESPONSE
COAGULATION
HYPOXIA
IL2_STAT5_SIGNALING
TGF_BETA_SIGNALING
KRAS_SIGNALING_UP
HEDGEHOG_SIGNALING
ALLOGRAFT_REJECTION
-log(p-value)
E
HALLMARK Enrichment in CAFs (Co-culture v.s. Monoculture)
TGF_BETA_SIGNALING
APICAL_JUNCTION
UV_RESPONSE_DN
MITOTIC_SPINDLE
G2M_CHECKPOINT
WNT_BETA_CATENIN_SIGNALING
ANDROGEN_RESPONSE
EMT
MYOGENESIS
E2F_TARGETS
-log(p-value)
D
TF activity
Mono_Cancer
Co-Cancer
HIF1A
EGR1
ATF2
EPAS1
SP1
JUN
RARA
STAT3
FOXL2
PAX6
F
panCAF
myCAF
iCAF
apCAF
THBS2
TPM1
FAP
-log (p-value)
Monoculture
logFC
Co-culture

Figure S6. Co-cultivation of CAFs and chemoresistant OCCC cells *in vitro* recapitulates the chemoresistant niche. Related to Figure 5.

(A) Western blot analysis of established cancer cells (OVN-48) and CAFs.

(B) UMAP feature plots of cancer & CAF markers in the cultivated cells shown in Figure 6G.

(C) Bar chart showing enrichment of specific biological pathways in cancer cells in the presence of CAFs. Enrichment of a pathway is calculated by comparing the average ssGSEA values of HALLMARK gene sets in cancer cells under co-culture and monoculture conditions. *P*-values of the top 10 terms enriched in cancer cells co-cultured with CAFs are shown.

(D) Heatmap of normalized TF activity in cancer cells under monoculture and co-culture conditions. The VIPER scores for the Top 10 TF genes activated in the Cancer #2 subpopulation (Figure S2C) are shown. There was no detectable expression of PAX6 in cancer cells, and its VIPER score was not calculated.

(E) Bar chart showing enrichment of specific biological pathways in CAFs in the presence of cancer cells. Enrichment of a pathway is calculated by comparing the average ssGSEA values of HALLMARK gene sets in CAFs under co-culture and monoculture conditions. *P*-values for the top 10 terms enriched in CAFs under co-culture conditions are shown.

(F) Volcano plots showing preferential induction of myCAF signature genes in CAFs co-cultured with cancer cells. The average expression values for the CAF signature genes (shown in Figure 5E) in CAFs under monoculture and co-culture conditions were calculated, and relative ratios are shown. The horizontal and vertical axes represent $\log_{10}$ -fold changes and *p*-values, respectively. Red dots: myCAF signature genes; Yellow dots: iCAF signature genes; Green dots: apCAF signature genes; Black dots: panCAF signature genes. A list of signature genes is presented in Table S3. *P*-values were determined by Student's t test.

A

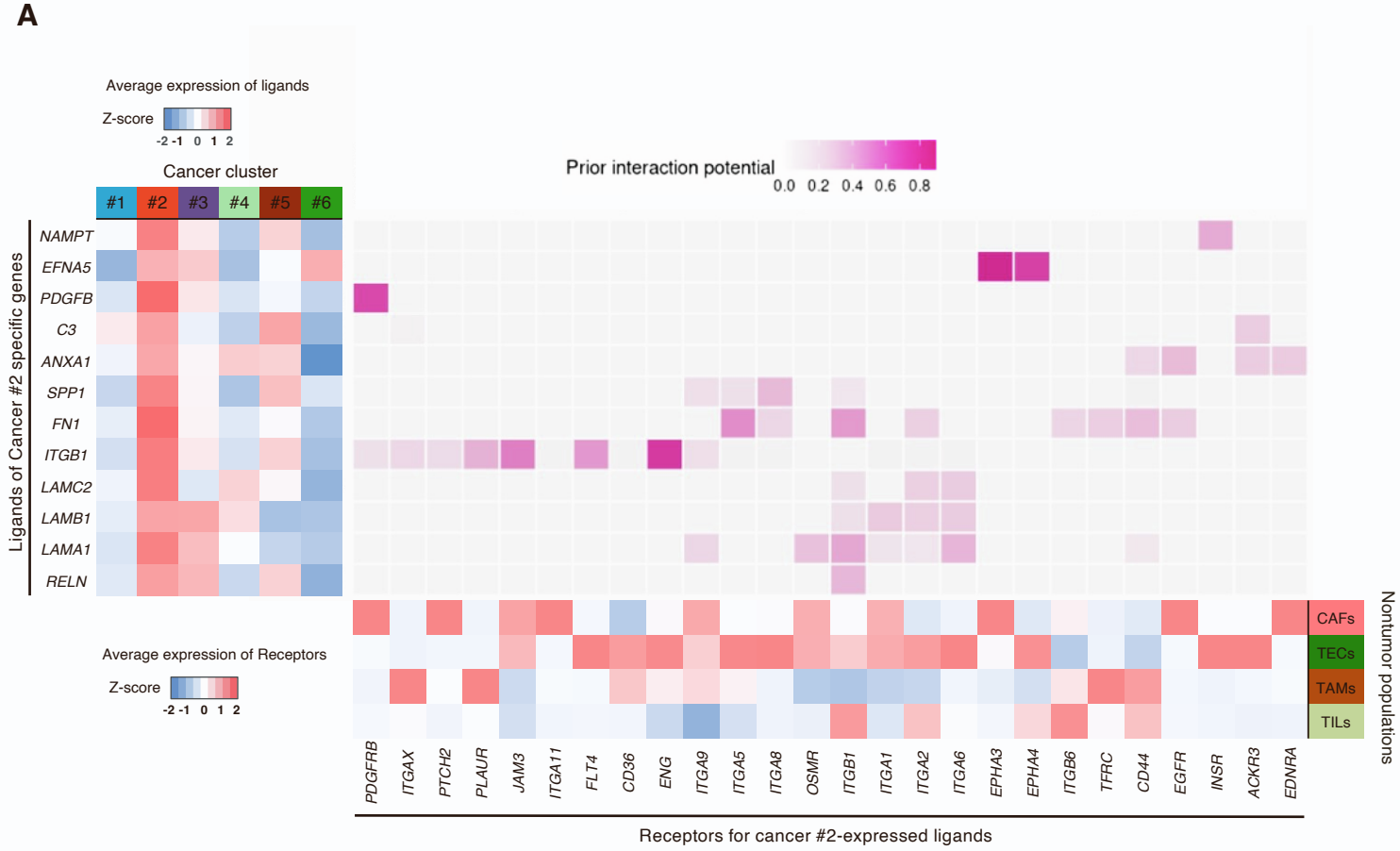
Average expression of ligands
Z-score
-2 -1 0 1 2
Cancer cluster
#1 #2 #3 #4 #5 #6
Ligands of Cancer #2 specific genes
NAMPT
EFNA5
PDGFB
C3
ANXA1
SPP1
FN1
ITGB1
LAMC2
LAMB1
LAMA1
RELN
Prior interaction potential
0.0 0.2 0.4 0.6 0.8
Average expression of Receptors
Z-score
-2 -1 0 1 2
CAFs
TECs
TAMs
TILs
Nontumor populations
PDGFRB
ITGAX
PTCH2
PLAUR
JAM3
ITGA11
FLT4
CD36
ENG
ITGA9
ITGA5
ITGA8
OSMR
ITGB1
ITGA1
ITGA2
ITGA6
EPHA3
EPHA4
ITGB6
TFRC
CD44
EGFR
INSR
ACKR3
EDNRA
Receptors for cancer #2-expressed ligands

B

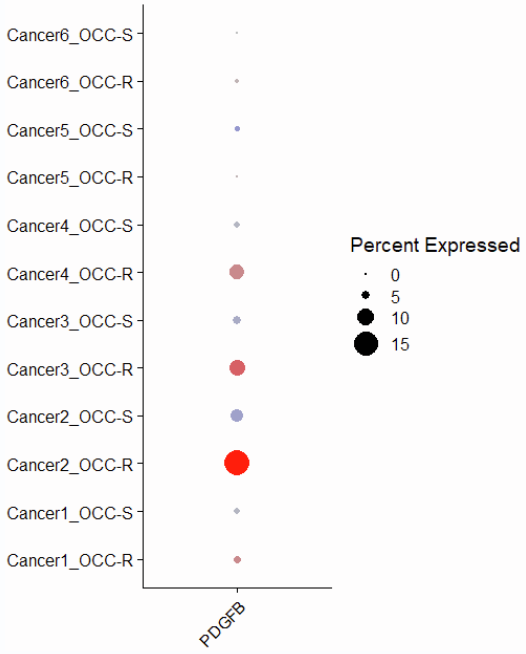
Cancer6_OCC-S
Cancer6_OCC-R
Cancer5_OCC-S
Cancer5_OCC-R
Cancer4_OCC-S
Cancer4_OCC-R
Cancer3_OCC-S
Cancer3_OCC-R
Cancer2_OCC-S
Cancer2_OCC-R
Cancer1_OCC-S
Cancer1_OCC-R
PDGFB
Percent Expressed
0
5
10
15

C

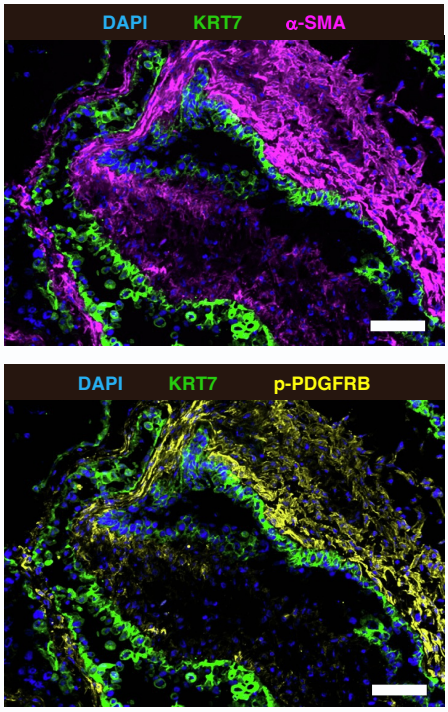
DAPI KRT7 α-SMA
DAPI KRT7 p-PDGFRB

Figure S7. CAF activation by cancer-derived PDGF mediates chemoresistance and HIF-1a expression of cancer cells. Related to Figure 6.

(A) Prediction of possible interactions between Cancer #2-expressed ligands and CAF-expressed receptors by using NicheNet. (Left matrix) heatmap showing expression of top-ranking ligands that are preferentially expressed in the Cancer #2 subpopulation. (Bottom matrix) heatmap showing corresponding receptors expressed in nontumor populations. (Middle) heatmap showing the potential interactions between ligand-receptor pairs between the Cancer #2 subpopulation and nontumor cells, which are based upon prior knowledge of signaling and gene regulatory networks predicted by NicheNet.

(B) Dot plots showing average expression of *PDGFB* in the indicated cancer subpopulations from the chemoresistant and chemosensitive cases

(C) Representative images of co-immunostaining of frozen sections of chemoresistant tumor (OCC-R3) with the indicated antibodies.

A

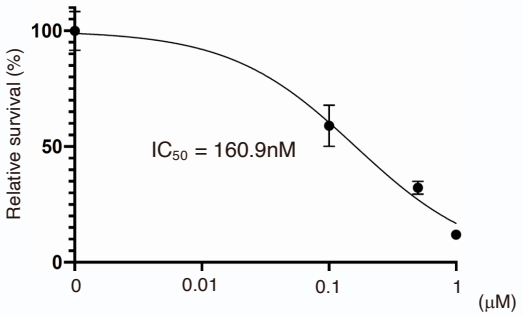
100
50
0
Relative survival (%)
IC50 = 160.9nM
0
0.01
0.1
1
(μM)

B

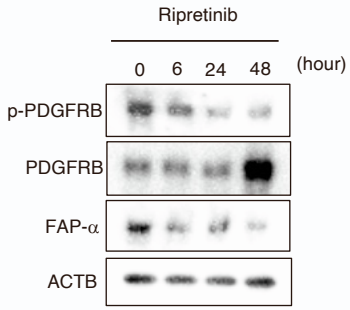
Ripretinib
0 6 24 48 (hour)
p-PDGFRB
PDGFRB
FAP-α
ACTB

C

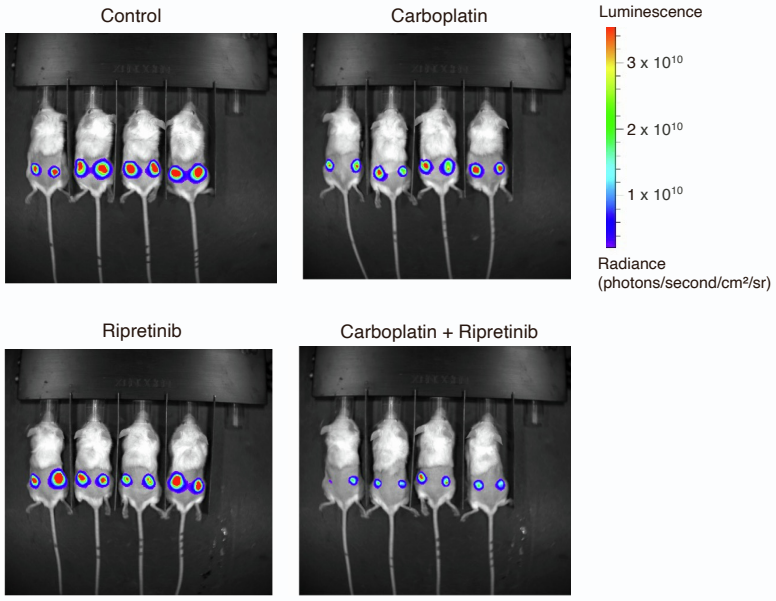
Control
Carboplatin
Luminescence
3 x 10^10
2 x 10^10
1 x 10^10
Radiance
(photons/second/cm²/sr)
Ripretinib
Carboplatin + Ripretinib

D

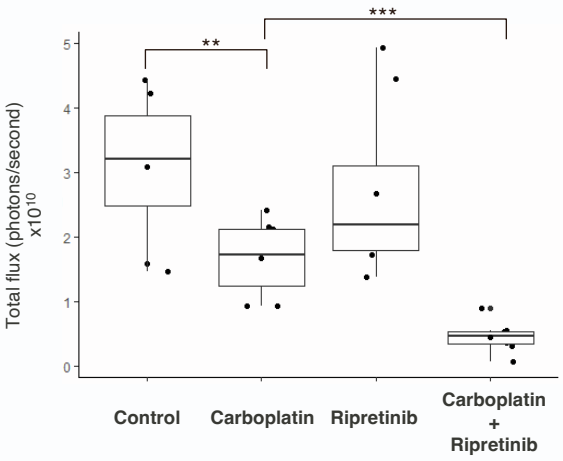
**
***
Total flux (photons/second)
x10^10
Control
Carboplatin
Ripretinib
Carboplatin
+
Ripretinib

E

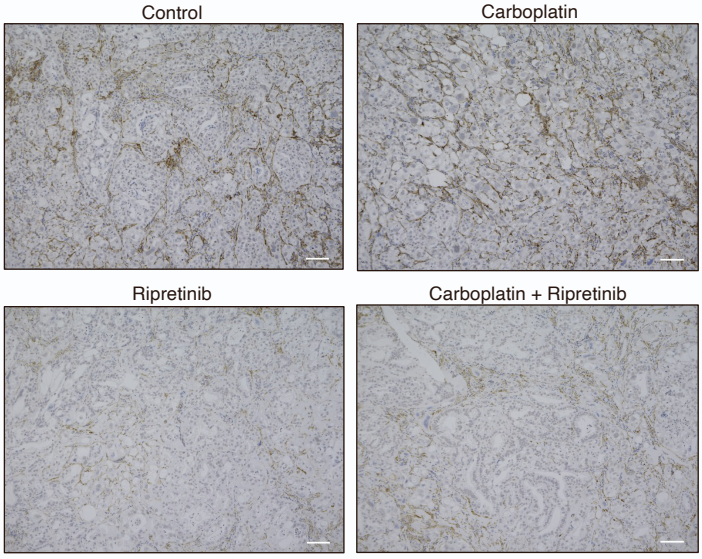
Control
Carboplatin
Ripretinib
Carboplatin + Ripretinib

F

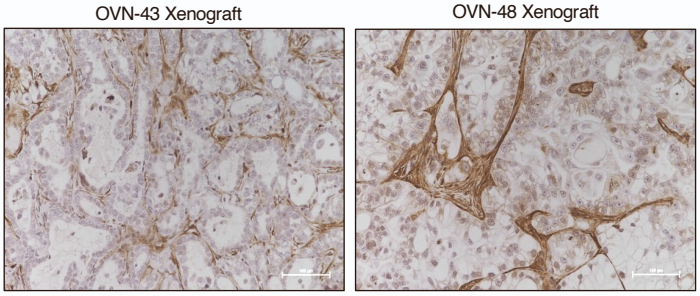
OVN-43 Xenograft
OVN-48 Xenograft

G

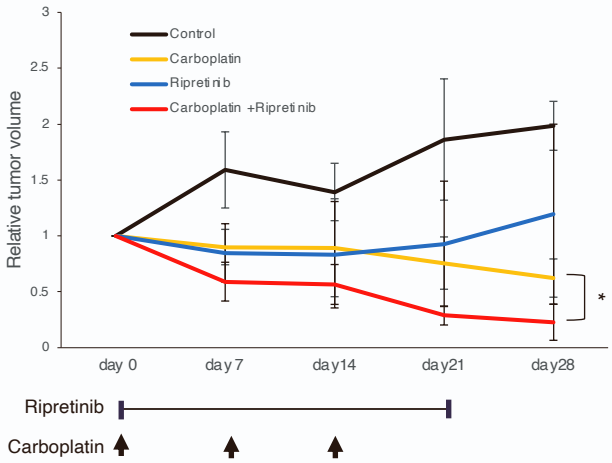
Control
Carboplatin
Ripretinib
Carboplatin +Ripretinib
Relative tumor volume
day 0
day 7
day14
day21
day28
*
Ripretinib
Carboplatin

Figure S8. CAF inhibition by Ripretinib in combination with Carboplatin blocks tumor growth of OCCC. Related to Figure 7.

(A) Dose-response curve of the CAFs treated with Ripretinib for 7 days.

(B) Western blot analyses of CAFs treated with 1μM Ripretinib for the indicated times.

(C) Bioluminescence images of luciferase activity in tumor xenografts treated as indicated (4 weeks after chemotherapy).

(D) Box plots of the luciferase activity shown in b, calculated by measuring total flux from the tumors. *P*-values were determined by Student's t test.

(E) Immunostaining of the tumor xenografts shown in C with an α-SMA antibody. Scale bars, 100 μm. Statistically significant differences are indicated: $^{**}p < 0.01$, $^{***}p < 0.001$.

(F) α-SMA Immunostaining of the xenografted tumors after injection of the indicated cancer spheroid cells alone. Scale bars: 100 μm.

(G) Xenografted tumors (OVN-43, 77 days after transplantation of cancer cells) were treated with the indicated combination of Carboplatin and/or Ripretinib, and tumor volumes were measured every week. The data are presented as mean ± SD (n=3). P-values were determined by Student's t test. $^{*}p < 0.05$.